Improving Open Circuit Potential in Hybrid P3HT:CdSe Bulk Heterojunction Solar Cells *via* Colloidal *tert*-Butylthiol Ligand Exchange

Matthew J. Greaney, Saptaparna Das, David H. Webber, Stephen E. Bradforth, and Richard L. Brutchey*

Department of Chemistry and the Center for Energy Nanoscience, University of Southern California, Los Angeles, California 90089-0744, United States

ABSTRACT Organic ligands have the potential to contribute to the reduction potential, or lowest unoccupied molecular orbital (LUMO) energy, of semiconductor nanocrystals. Rationally introducing small, strongly binding, electron-donating ligands should enable improvement in the open circuit potential of hybrid organic/inorganic solar cells by raising the LUMO energy level of the nanocrystal acceptor phase and thereby increasing the energy offset from the polymer highest occupied molecular orbital (HOMO). Hybrid organic/inorganic solar cells fabricated from blends of *tert*-butylthiol-treated CdSe nanocrystals and poly(3-hexylthiophene) (P3HT) achieved power conversion efficiencies of 1.9%. Compared to devices made from pyridine-treated and nonligand exchanged CdSe, the thiol-treated CdSe nanocrystals are found to consistently exhibit the highest open circuit potentials with V_{OC} = 0.80 V. Electrochemical determination of LUMO levels using cyclic voltammetry and spectroelectrochemistry suggest that the thiol-treated CdSe nanocrystals possess the highest lying LUMO of the three, which translates to the highest open circuit potential. Steady-state and time-resolved photoluminescence quenching experiments on P3HT:CdSe films provide insight into how the thiol-treated CdSe nanocrystals also achieve greater current densities in devices relative to pyridine-treated nanocrystals, which are thought to contain a higher density of surface traps.

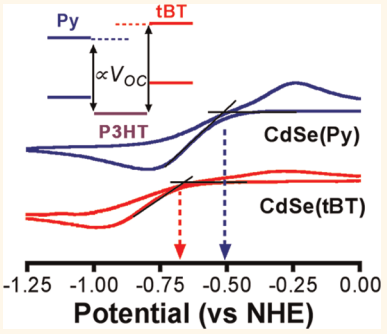

KEYWORDS: CdSe · semiconductor nanocrystal · P3HT · hybrid solar cell · open-circuit potential

Organic photovoltaics (OPVs) are attractive candidates for third generation solar cell technologies because they can be inexpensively solution processed (*e.g.*, allowing roll-to-roll printing), in addition to having the added benefits of being thin and flexible if the appropriate substrates are used.[1−4] The most commonly employed bulk heterojunction (BHJ) geometry consists of an active layer wherein a conjugated polymer donor is blended with a fullerene acceptor.[5,6] Such types of OPVs have achieved power conversion efficiencies (PCEs) of $\eta_P = 8.3\%$.[7] Hybrid organic/inorganic solar cells utilize inorganic semiconductor nanocrystals as the acceptor component. Semiconductor nanocrystals possess several attributes that should make them attractive substitutes for fullerene acceptors; namely, (i) tunable band gaps and energy levels through compositional control and quantum confinement effects, (ii) strong, broad absorption at energies higher than the band edge, (iii) high dielectric constants to help overcome the strong exciton binding energy of conjugated polymers, and (iv) high electron mobilities relative to organic materials.[8−12] In addition, the interfacial band structure of semiconductor nanocrystals can potentially be synthetically tuned.[13,14] Although the PCEs of hybrid organic/inorganic solar cells currently lag behind their all-organic counterparts, theoretical efficiencies of η_P >12% should be attainable for conjugated polymer/CdSe solar cells that utilize donor polymers with band gaps between 1.5 and 1.6 eV and HOMO energies near −4.8 eV relative to vacuum.[12,15]

Since the seminal work of Huynh, Dittmer, and Alivisatos in 2002 that described poly(3-hexylthiophene) (P3HT):CdSe nanocrystal-based BHJ devices,[16] the P3HT:CdSe system has been used as a model for hybrid organic/inorganic solar cells. The current record efficiency for a P3HT:CdSe BHJ device stands at $\eta_P = 2.6\%$, which used 65-nm long CdSe nanorods as the acceptor phase.[17] The anisotropic nature of the CdSe nanorods resulted in increased current densities by facilitating electron transport along the principal rod axis, thereby reducing the number of electron hopping events between individual nanocrystals required for charge collection. This design criterion has also been demonstrated to work with other

* Address correspondence to brutchey@usc.edu.

Received for review February 20, 2012 and accepted April 26, 2012.

Published online April 26, 2012
10.1021/nn3007509

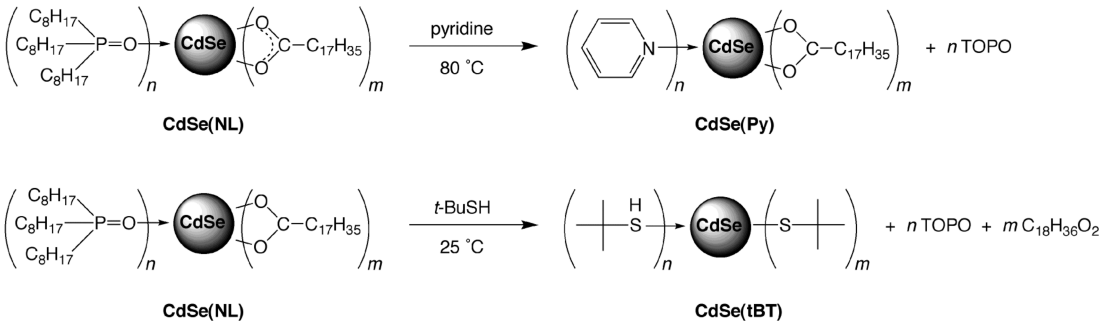

Scheme 1. Ligand exchange of as-prepared CdSe(NL) nanocrystals with pyridine (Py) and *tert*-butylthiol (tBT). A more complete ligand exchange is achieved with a thiol as compared to pyridine.

anisotropic CdSe morphologies, such as tetrapods and hyperbranched structures.[18−20] A second means through which the efficiency of hybrid organic/inorganic solar cells can be improved is to utilize lower band gap polymers to maximize absorption at wavelengths longer than 640 nm (*i.e.*, the absorption edge of P3HT). Along these lines, Dayal *et al*. first utilized a conjugated low band gap polymer (PCPDTBT, $E_g \approx$ 1.4 eV) in conjunction with anisotropic CdSe tetrapods to achieve champion efficiencies of $\eta_P = 3.2\%$.[21] More recently, Jeltsch *et al*. have combined PCPDTBT with a mixture of 0-D and 1-D CdSe nanocrystals to achieve efficiencies of $\eta_P = 3.6\%$.[22] Here, it is thought that parallel oriented CdSe nanorods are percolated through the active layer with CdSe quantum dot interconnects to more efficiently collect charge.

One design criterion that can be used to improve hybrid organic/inorganic BHJ cells that is unique to these systems is the ability to molecularly tune the donor/acceptor interface with organic ligands on the surface of the inorganic nanocrystals using simple coordination chemistry.[22−26] Up to this point, the principal rationale behind this concept has been to remove the large and insulating native (or legacy) ligands from the nanocrystal surface to better facilitate charge transfer between the donor and acceptor and charge collection from the nanocrystal phase. This has been achieved to varying degrees of success by exchanging the native ligands with small molecules, such as, pyridine, butylamine, and hexanoic acid.[21,22,27−30] In all cases, the short circuit current (J_{SC}) of the resulting devices increased considerably relative to devices prepared with the native ligand remaining on the nanocrystal surface, achieving short circuit current densities up to 6 mA cm^{-2} for ligand exchanged P3HT:CdSe quantum dot based BHJ devices.[30] Inherent to this ligand exchange process is the creation or removal of surface trap states on the nanocrystal, which will also contribute to the efficiency of charge collection. Herein we consider another effect, which is the potential for ligands to contribute to the highest occupied molecular orbital/lowest unoccupied molecular orbital (HOMO/LUMO) energies of the semiconductor nanocrystal. This could have important consequences for device performance since V_{OC} is directly proportional to the energy offset (ΔE_{DA}) between the HOMO of the donor polymer and the LUMO of the nanocrystal acceptor.[1,5,31] If the LUMO energy of the semiconductor nanocrystal can be increased relative to the HOMO of the conjugated polymer *via* facile ligand exchange, then this would be yet another avenue to increase the device performance of organic/inorganic hybrid solar cells.

We report an increase in device performance for P3HT:CdSe BHJ solar cells through a colloidal ligand exchange of CdSe nanocrystals with *tert*-butylthiol (*t*-BuSH, tBT).[32] While the ligand exchange with tBT results in increased J_{SC} and external quantum efficiency (EQE) as a result of the more effective removal of insulating native ligands when compared to pyridine (Py) exchange (Scheme 1), we also observed an increase in V_{OC} as a result of the tBT raising (making less negative) the level of the CdSe nanocrystal LUMO relative to the HOMO of P3HT. A combination of thermogravimetric analysis, Fourier transform infrared (FT-IR) spectroscopy, (spectro)electrochemistry, steady-state and time-resolved photoluminescence spectroscopy, and device measurements are used to elucidate the role that the tBT ligand plays on the interfacial effects and device performance of model P3HT:CdSe BHJ devices.

RESULTS AND DISCUSSION

Colloidal Ligand Exchange. The CdSe nanocrystals were prepared according literature protocol,[33] in the presence of stearic acid and as-received tri-*n*-octylphosphine oxide (TOPO), which is known to contain phosphonic acid impurities. The nanocrystals were purified by washing four times using toluene as the dispersant and ethanol as the flocculant. The as-prepared CdSe nanocrystals possess negatively charged and strong binding native ligands (NLs; *i.e.*, stearate, alkylphosphonates) that originate from the synthetic preparation. The resulting CdSe(NL) nanocrystals were 4.5 nm in diameter, as evidenced by a clear first exciton peak of 600 nm in the UV−vis absorption spectrum (see Supporting Information, Figure S1) of a nanocrystal dispersion in toluene.[33] A photoluminescence

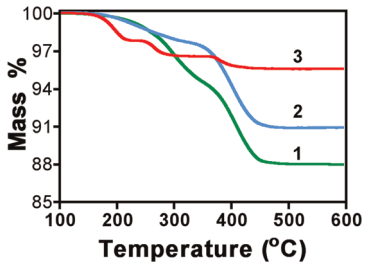

Figure 1. TGA traces of CdSe(NL) (1), CdSe(Py) (2), and CdSe(tBT) (3) obtained under flowing nitrogen with a ramp rate of 10 °C min^{-1}. The % mass losses for CdSe(NL), CdSe(Py), and CdSe(tBT) were 12.0, 9.6, and 4.4%, respectively.

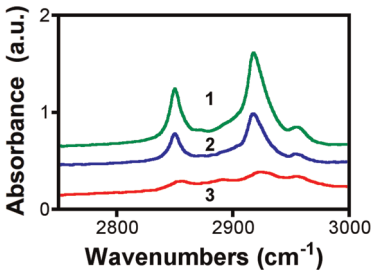

Figure 2. FT-IR spectra of CdSe(NL) (1), CdSe(Py) (2), and CdSe(tBT) (3). The spectra were normalized to the 2089 cm^{-1} ν(CN) stretching peak of a measured $Fe_4[Fe(CN)_6]_3$ internal standard (not shown). The spectra are offset for clarity.

spectrum (see Supporting Information, Figure S1) was obtained using an excitation wavelength of 550 nm; it displayed a clear near-band edge emission at λ_{max} = 635 nm. Transmission electron microscopy (TEM) analysis confirmed that the CdSe(NL) nanocrystals were quasispherical, with a mean diameter of 4.2 ± 0.5 nm (see Supporting Information, Figure S2), in agreement with the UV−vis absorption spectra.

Facile ligand exchange of the CdSe(NL) nanocrystals was carried out by rinsing the nanocrystals with tBT in tetramethyluruea (TMU) at room temperature, flocculating with methanol/pentane, and redispersing the final suspension in TMU with a small amount of tBT to act as an antioxidant.[32] The resulting CdSe(tBT) nanocrystals form suspensions in TMU at concentrations up to 100 mg mL^{-1} that are stable for several months when stored at 4 °C in the dark. During the tBT ligand exchange process, care was taken to avoid exposure to light to prevent formation of disulfides from photooxidation of tBT. For comparison, the CdSe(NL) nanocrystals were also exchanged with the prototypical Py ligand by stirring the as-prepared nanocrystals in neat pyridine at 80 °C, flocculating with pentane, and redispersing the final suspension of CdSe(Py) in pyridine at concentrations up to 80 mg mL^{-1}.

To characterize the efficacy of ligand exchange, the CdSe(Py) and CdSe(tBT) nanocrystals were analyzed using thermogravimetric analysis (TGA) and FT-IR spectroscopy and compared to the as-prepared CdSe(NL) sample. Figure 1 shows an overlay of the results obtained from typical TGA traces (ambient to 600 °C, 10 °C min^{-1}, under flowing nitrogen) for CdSe(NL), CdSe(Py), and CdSe(tBT) samples. It is evident that ligand exchange with both Py and tBT reduces the overall organic content on the CdSe nanocrystal surface. Taking the mass at 550 °C as approximating pure CdSe, it was found that CdSe(NL) nanocrystals typically contained 12.0% organic content by weight after purification by four toluene/ethanol washes. After ligand exchange with Py, the organic content is reduced to 9.1%, while exchange with tBT reduces the organic content to 4.4%, indicating a more efficient ligand exchange. Significantly, the mass loss event at ~400 °C, which is attributed to loss of strongly bound stearate and alkylphosphonates, is greatly reduced upon ligand exchange with tBT.[32] This suggests that the thiol is able to bind to the nanocrystal surface in the deprotonated thiolate form, thereby displacing the negatively charged stearate and alkylphosphonate ligands. In contrast, Py is unable to efficiently displace these negatively charged ligands. FT-IR spectroscopy provides further validation of the increased effectiveness of tBT over Py ligand exchange (Figure 2). A clear reduction in the ν(C−H) stretching intensity at 2850 and 2920 cm^{-1} is observed upon introduction of both ligands relative to the CdSe(NL) nanocrystals; however, ligand exchange with tBT results in a greater decrease in ν(C−H) stretching intensity as compared to Py treatment.

Electrochemical Characterization. Cyclic voltammetry (CV) was used to estimate the relative LUMO energies of the CdSe nanocrystals. Films of the CdSe(NL), CdSe(Py), and CdSe(tBT) nanocrystals were prepared by spin-casting nanocrystal suspensions onto ITO, drying the nanocrystal films under flowing nitrogen, and measuring them under identical nonaqueous conditions. An approximation of the effective energy of the LUMO levels can be obtained from the onset potential of CdSe nanocrystal reduction waves.[34−36] Correcting the measured onset values with respect to vacuum after calibration against the ferrocene/ferrocinium (Fc/Fc^+) redox couple, LUMO energies (relative to vacuum) are obtained according to[36,37]

$$E_{LUMO} = -(E_{red} + 4.5)\ \text{eV} \quad (1)$$

where E_{red} is the onset value of the reduction wave obtained from CV *versus* the normal hydrogen electrode (NHE). Although there is no apparent difference in the optical band gap after Py or tBT treatment, the reduction onset potential, and thus the position of the LUMO relative to vacuum, is shifted following ligand treatment (Figure 3). Based on the reduction peak onsets by CV, the energy of the LUMO levels are approximated as −3.93, −4.00, and −3.84 eV for CdSe(NL), CdSe(Py), and CdSe(tBT), respectively. The complete set of electrochemically and optically determined parameters for the CdSe nanocrystals and P3HT are given in Table 1. In addition, differential pulse

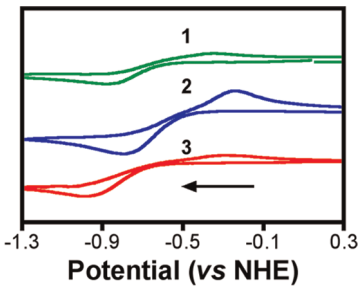

Figure 3. CV traces for CdSe(NL) (1), CdSe(Py) (2), and CdSe(tBT) (3) spun-cast onto ITO. Data were collected with a scan rate of 20 mV s^{-1} in 0.10 M TBAP with a Pt wire counter-electrode and Ag wire pseudo-reference-electrode calibrated against the Fc/Fc^{+} redox couple. All potentials are given relative to NHE. Reduction onset values of −0.57, −0.50, and −0.66 V were obtained for CdSe(NL), CdSe(Py), and CdSe(tBT), respectively.

TABLE 1. Optical Band Gaps and Electrochemically Determined HOMO/LUMO Levels for P3HT and CdSe Nanocrystals. CV Was Used for the Electrochemically Determined Values

	$E_{g,optical}$ (eV)	E_{red} (V)	E_{ox} (V)	E_{LUMO} (eV)	E_{HOMO} (eV)
P3HT	1.9	n/a	0.70	n/a	−5.25
CdSe(NL)	2.0	−0.57	n/a	−3.93	−5.93[a]
CdSe(Py)	2.0	−0.50	n/a	−4.00	−6.00[a]
CdSe(tBT)	2.0	−0.66	n/a	−3.84	−5.84[a]

[a] E_{HOMO} values were estimated by adding the optical band gap to the electrochemically determined E_{LUMO}.

voltammetry (DPV) was employed as a means of corroborating the trend in reduction potentials for CdSe following ligand exchange. On the basis of the reduction peak onsets measured by DPV, the energy of the LUMO levels are approximated as −3.86, −3.92, and −3.73 eV for CdSe(NL), CdSe(Py), and CdSe(tBT), respectively (see Supporting Information, Figure S3). These LUMO energies are all slightly less negative compared to those approximated by CV, but the absolute differences are similar, and the general trend is the same. The HOMO levels are more difficult to approximate by CV and DPV as a result of the appearance of peak shoulders under oxidizing conditions, which may be the result of trap states.[38]

To confirm the relative positioning of CdSe nanocrystal LUMO levels for the three samples, spectroelectrochemistry (SEC) was performed under reducing conditions. The lowest energy exciton peak, with an absorption λ_{max} = 600 nm, was monitored under increasing negative bias in a nonaqueous electrochemical cell. The UV−vis spectra of CdSe(NL), CdSe(Py), and CdSe(tBT) nanocrystal films collected at decreasing bias are compared in Figure 4. As the electrochemical reduction of the CdSe nanocrystals occurs, electrons are injected into the LUMO, which causes a bleach of the first exciton peak.[39,40] At potentials down to −500 mV (*vs* NHE), all three spectra are virtually unperturbed. At −590 mV, the CdSe(NL) nanocrystal film begins to exhibit a bleach of the first exciton peak intensity. Similar bleaching is observed for CdSe(Py) below −540 mV and for CdSe(tBT) below −740 mV. Using the potentials where bleaching is first observed, the LUMO energies can be approximated as −3.91, −3.96, and −3.76 eV for CdSe(NL), CdSe(Py), and CdSe(tBT), respectively. Although bleaching of the first exciton peak is not observed at potentials that exactly correspond to the reduction wave onsets from CV analysis, the deviation is <80 mV for all three samples and the general energy trend is in agreement with CV and DPV results. It is of interest to note that bleaching of the first exciton peak is reversible as long as the CdSe nanocrystals are not subjected to extremely reducing or oxidizing potentials, in which case the films undergo fatal degradation and delamination.

Hybrid Solar Cells. To investigate the effect of ligand treatment on photovoltaic performance, BHJ solar cells with a simple ITO/PEDOT:PSS/P3HT:CdSe/Al device architecture were studied. All devices were fabricated and tested in the ambient atmosphere without any thermal annealing. The device characteristics are summarized in Table 2, and *I*−*V* curves are given in Figure 5. In each case, an 8:1 weight ratio of CdSe nanocrystals to polymer was used, with active layer thicknesses between 65 and 75 nm, as determined by X-ray reflectivity measurements. As expected, the CdSe(NL) acceptor produces the lowest efficiency solar cells, primarily due to low current densities and poor fill factors (FF). This can be rationalized by considering the insulating nature of the ligand shell from the high organic content, as determined by TGA. Considering the ambient processing conditions and lack of thermal treatment, devices based on CdSe(Py) acceptors give reasonable efficiencies of η_P = 1.0%. An increase in J_{SC} (3.69 mA cm^{-2}) and FF (0.47) relative to devices using CdSe(NL) acceptors can be explained by the reduced barrier to interfacial charge transfer facilitated by the smaller Py ligand shell and overall reduced organic content.[27] The V_{OC} for devices using CdSe(Py) acceptors (0.57 V) is significantly less than those with CdSe(NL) acceptors (0.70 V). Comparatively, the best P3HT:CdSe solar cells result from devices using CdSe(tBT) acceptors and demonstrate PCEs of 1.9%. These devices have the highest J_{SC} (5.6 mA cm^{-2}) and V_{OC} (0.80 V), although there tends to be a slight decrease in FF between CdSe(Py) and CdSe(tBT). Based on the electrochemically determined LUMO energies for the three types of CdSe nanocrystal acceptors, the observed V_{OC} values directly correlate with the energy level offset (*i.e.*, ΔE_{DA}) between the HOMO energy of P3HT and the LUMO energy of CdSe. For OPVs, it is often observed that the theoretical maximum V_{OC} is dependent on the energy level difference between the HOMO of the donor material and the LUMO of the acceptor material.[1,5,31] In addition to the dependence of V_{OC} on ΔE_{DA}, Potscavage *et al.* have

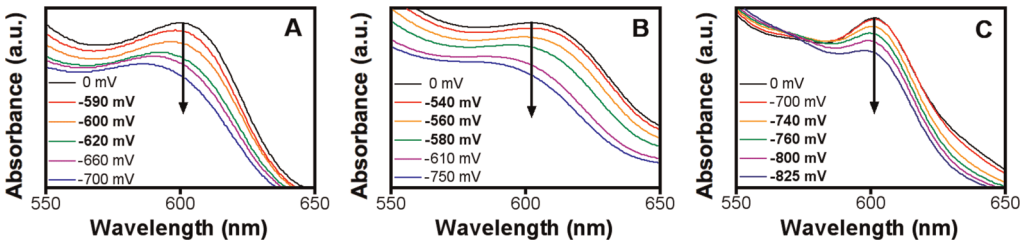

Figure 4. Visible absorption spectra for CdSe(NL) (A), CdSe(Py) (B), and CdSe(tBT) (C) spun-cast onto ITO collected with decreasing applied bias. Data were acquired under nitrogen in 0.10 M TBAP using a Pt wire counter-electrode and Ag wire pseudo-reference-electrode calibrated against the Fc/Fc^+ redox couple. All potentials are listed relative to NHE. Visible absorption spectra were obtained after a 2 min equilibration period following each potential step. Initial exciton bleaching is first observed at −0.54, −0.59, and −0.74 V for CdSe(NL), CdSe(Py), and CdSe(tBT), respectively.

TABLE 2. Short-Circuit Current (J_{SC}), Open Circuit Voltage (V_{OC}), Fill Factor (FF), and Power Conversion Efficiency (η_P) for P3HT:CdSe Devices under Simulated AM 1.5G Light Illumination. The HOMO/LUMO Energy Offset Determined by CV ($\Delta E_{DA,CV}$) for P3HT and CdSe with each Ligand Is Given for Comparison

acceptor ligand	J_{SC} (mA cm^{-2})	V_{OC} (V)	FF	η_P (%)	$\Delta E_{DA,CV}$ (eV)
NL	1.95	0.70	0.36	0.5	1.27
Py	3.69	0.57	0.47	1.0	1.20
tBT	5.62	0.80	0.43	1.9	1.36

shown an inverse relationship between V_{OC} and the reverse saturation current (J_O).[41] To confirm that the V_{OC} differences in our hybrid solar cells were in fact due to changes in ΔE_{DA} and not to J_O, the dark $I-V$ curves for P3HT:CdSe(NL), P3HT:CdSe(Py), and P3HT:CdSe(tBT) were compared and no significant differences in J_O were observed (see Supporting Information, Figure S4). Since P3HT is used as the donor material for all of the devices (with an electrochemically measured HOMO energy of −5.20 eV; see Supporting Information, Figure S5), the relative differences in V_{OC} can be attributed to the nanocrystal LUMO energy differences induced by ligand exchange.

Several groups have observed a dependence of nanocrystal frontier energy levels on surface ligands, with shifts up to 0.25−0.57 eV observed upon a change in ligand.[24,26,39,42,43] While the dipole moment of organic ligands has been shown to influence the energy levels of 2-D semiconductor surfaces at the interface,[44] no such correlation between the frontier energy level shift and the magnitude or sign of ligand dipole has yet been established for 0-D semiconductor nanocrystals.[24,42] Even though the ligand dipole may not have a clear effect on the frontier energy levels, it has been suggested that the anchoring group of the ligand may play a more important role in frontier energy level shifts.[42] Interestingly, Jasieniak *et al.* reported a lower lying HOMO for CdSe(Py) than CdSe(alkane thiol) using photoelectron spectroscopy in air,[43] which agrees with the trend measured here for the LUMO energies of CdSe(Py) and CdSe(tBT). It is important to consider that because the ligand exchange reactions are not always quantitative (*vide supra*), the resulting nanocrystal may contain a mixed ligand shell with an

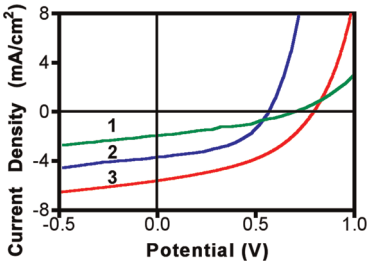

Figure 5. $I-V$ curves for devices with ITO/PEDOT:PSS/P3HT:CdSe/Al structure, made with CdSe(NL) (1), CdSe(Py) (2), or CdSe(tBT) (3) nanocrystal acceptors. Device areas were 0.8 mm^2.

electronic structure influenced by many factors contributing to the frontier energy levels.

The J_{SC} values measured from $I-V$ curves were confirmed by integrated EQE data. Figure 6A shows an overlay of the EQE data for devices with the three different CdSe acceptors. The corresponding absorption spectra for neat P3HT, CdSe(tBT), and hybrid P3HT:CdSe(tBT) films are given in Figure 6B. The EQE and absorption spectra indicate that the P3HT and CdSe nanocrystals both contribute to the generated photocurrent. In agreement with $I-V$ data, devices with the CdSe(tBT) acceptors gave the highest photocurrents with peak EQEs greater than 35% at 430 nm. While the absorption features of P3HT overlap with the characteristic first exciton peak of the CdSe nanocrystals, the increasing photocurrent below 500 nm is indicative of contribution by the nanocrystals.

The differences in V_{OC} can be rationalized based on the (spectro)electrochemical data, but the source of the differences in J_{SC} for the hybrid devices with the three CdSe(NL), CdSe(Py), and CdSe(tBT) acceptors is less clear. Lower overall organic content in the nanocrystal ligand sphere is expected to facilitate greater photocurrent, consistent with the trend demonstrated by a combination of TGA and device data. However, it is known that the density of traps and/or defect sites on the surface of semiconductor nanocrystals can also affect photoinduced charge carrier lifetime and recombination probability.[8,9,45] While extending the charge carrier lifetimes can be beneficial for harvesting, it can significantly impede charge transfer and hamper

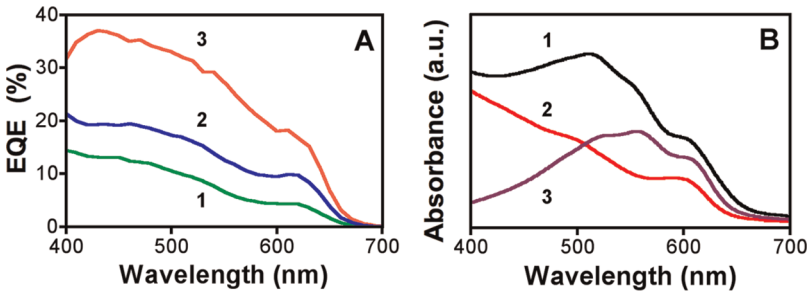

Figure 6. (A) EQE spectra for hybrid solar cells fabricated with P3HT:CdSe(NL) (1), P3HT:CdSe(Py) (2), and P3HT:CdSe(tBT) (3). (B) UV−vis absorption spectra of 1:8 (w/w) ratio P3HT:CdSe(tBT) (1), neat CdSe(tBT) (2), and neat P3HT (3) films on glass. The neat P3HT and CdSe(tBT) were spun-cast from *o*-dichlorobenzene solutions of 2.5 mg mL^{-1} P3HT and 20 mg mL^{-1} CdSe(tBT), respectively.

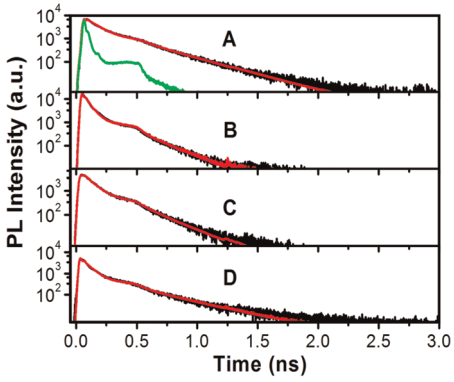

Figure 7. PL decay measurements with the corresponding fitted curves (λ_{ex} = 550 nm; λ_{em} = 650 nm) for neat P3HT (A) and P3HT blended with CdSe(NL) (D), CdSe(Py) (C), and CdSe(tBT) (B). For the hybrid films, data were fit with a sum of two exponential functions, whereas for neat P3HT one exponential function was used. PL lifetimes in the hybrid films were calculated using a weighted average to be 160 ps for P3HT:CdSe(NL), 110 ps for P3HT:CdSe(Py), and 90 ps for P3HT:CdSe(tBT). The lifetime of the neat P3HT film is 280 ps. The raw data are shown in black, and the fit results to the data are shown in red. The instrument response of the TCSPC apparatus is shown in green. The fitting parameters for the hybrid films are given in Table S1.

device performance if the extension is due to carrier trapping.[46,47] To probe the dynamics of charge transfer or energy transfer between the P3HT donor and the CdSe nanocrystal acceptor, a series of steady-state and time-resolved photoluminescence (PL) quenching studies were performed on the three hybrid blends. Samples were prepared with the same 8:1 wt/wt ratio of CdSe to P3HT and under identical processing conditions to the working devices. From the steady-state PL spectra for neat P3HT and hybrid films with the three CdSe nanocrystal acceptors (see Supporting Information, Figure S6) it is clear that CdSe(Py) and CdSe(tBT) nanocrystal acceptors result in enhanced quenching of the P3HT fluorescence when compared to the CdSe(NL) acceptor, with approximately 85% and 90% quenching efficiency of the 635 nm peak P3HT emission (λ_{ex} = 550 nm) for blends of P3HT:CdSe(Py) and P3HT:CdSe(tBT), respectively, compared to just 65% quenching efficiency for films of P3HT:CdSe(NL). The steady-state PL quenching suggests that charge transfer or energy transfer between the P3HT and nanocrystal phases is most efficient for the CdSe(Py) and CdSe(tBT) acceptors; however, interpretation of the steady-state data can be complicated by variations in sample thickness and orientation within the instrument. These complications can be avoided through the use of time-resolved photoluminescence measurements. The PL lifetime decay plots of hybrid films with the three CdSe(NL), CdSe(Py), and CdSe(tBT) nanocrystal acceptors are compared in Figure 7 (λ_{em} = 650 nm; λ_{ex} = 550 nm). On the basis of the neat absorption spectra for P3HT and CdSe(tBT), approximately 70% of light absorption at 550 nm stems from P3HT with the remaining absorption due to CdSe(tBT). Although both P3HT and CdSe nanocrystals absorb at 550 nm, the PL lifetime measurements on hybrid films largely monitor the decay of emission from the donor polymer since the steady-state emission line shape resembles that of P3HT (see Supporting Information, Figure S6).

As expected from the steady-state PL results, significant reduction of the P3HT PL lifetime is observed for hybrid blends with all three CdSe acceptors. The lifetime of a neat P3HT film was determined to be τ = 280 ps. For the hybrid films, the data cannot be fit with a single exponential, but it is most useful to characterize an average or weighted lifetime. (Weighted average lifetime was calculated using $\tau = (\sum_i a_i t_i^2)/(\sum_i a_i t_i)$, where a_i and t_i correspond to the amplitudes and time constants of individual exponents, respectively. (Berberan-Santos, M. N.; Bodunov, E. N.; Valeur, B. Mathematical Functions for the Analysis of Luminescence Decays with Underlying Distributions: 2. Becquerel (Compressed Hyperbola) and Related Decay Functions. *Chem. Phys.* **2005**, *317*, 57).) For P3HT:CdSe(NL) the average PL lifetime was τ = 160 ps, whereas for P3HT:CdSe(Py) and P3HT:CdSe(tBT) the average lifetimes were τ = 110 and 90 ps, respectively. This suggests that compared to P3HT:CdSe(NL), the quenching of P3HT PL is more efficient when the nanocrystals are treated with Py or tBT ligands, again indicating more efficient charge transfer or energy transfer for nanocrystals containing a diminished ligand shell. On the basis of the measured average luminescence lifetimes, an approximate P3HT PL quenching rate can be computed

ignoring inhomogeneities in the quenching; for CdSe-(NL), CdSe(Py), and CdSe(tBT) this quenching measure is 2.6, 5.3, and 7.2 ns^{-1}, respectively. For CdSe(tBT) the quenching rate is almost three times greater than with the CdSe(NL) acceptor, and nearly two times greater than for the CdSe(Py) acceptor.

From the time-resolved and steady-state PL spectra obtained for hybrid films, CdSe(tBT) seems to enable more efficient charge transfer or energy transfer than CdSe(Py) from P3HT based on the shorter luminescence lifetime. Furthermore, devices fabricated from CdSe(tBT) acceptors consistently exhibit higher J_{SC} and EQE than those made from CdSe(Py) acceptors. We suspected that differences in hybrid film morphologies could in part be responsible for the superior behavior of the P3HT:CdSe(tBT) films. However, investigation by TEM and AFM revealed little indication of morphological differences between P3HT:CdSe(Py) and P3HT:CdSe(tBT) films, suggesting another cause for the increased current densities (see Supporting Information, Figures S7, S8). The PL lifetime decay curves of neat CdSe(NL), CdSe(Py), and CdSe(tBT) nanocrystal films (λ_{em} = 650 nm; λ_{ex} = 400 nm) are given in Figure S9. The weighted average radiative lifetimes are determined as τ = 1.4, 3.3, and 4.4 ns for CdSe(NL), CdSe(Py), and CdSe(tBT), respectively. Assuming trap states hamper the radiative recombination of holes and electrons, it seems plausible that semiconductor nanocrystals with the greatest density of traps will exhibit the shortest PL lifetimes. Thus, due to the more efficient charge transfer or energy transfer between P3HT and CdSe(tBT), as compared to CdSe(Py), as well as a greater density of trap states in the CdSe(Py) nanocrystals, the extraction of charges from P3HT:CdSe(Py) based devices is more difficult (as reflected by a lower J_{SC} and integrated EQE) than for P3HT:CdSe(tBT) devices.

CONCLUSIONS

We fabricated hybrid solar cells that utilize CdSe nanocrystals ligand exchanged with the small, strongly binding, and electron donating tBT ligand. P3HT:CdSe-(tBT) devices demonstrate efficiencies of 1.9% and a maximum V_{OC} of 0.80 V. The high open circuit potential associated with devices using the CdSe(tBT) acceptors is attributed to an elevated nanocrystal LUMO energy relative to the HOMO energy of P3HT, which produces the greatest ΔE_{DA} of the three ligand types investigated. While the ability to tune the LUMO level of CdSe nanocrystals by various ligand treatments has been previously reported, we have, for the first time, demonstrated a direct correlation between the ligand-induced LUMO energy shift and the observed open circuit potential in operable solar cells. Excellent solution stability and processability, ambient atmosphere fabrication, and high overall performance render the tBT ligand system attractive for future hybrid solar cell applications.

EXPERIMENTAL METHODS

General Considerations. $CdCO_3$ (99.998% metals basis, "Puratronic" grade, Alfa Aesar), selenium (200 mesh powder, 99.999% metals basis, Alfa Aesar,), tri-*n*-octylphosphine oxide (TOPO, 98%, Alfa Aesar), tri-*n*-octylphosphine (TOP, ≥97%, Strem), stearic acid (95%, Sigma-Aldrich), 2-methyl-2-propanethiol (*tert*-butylthiol, tBT, 99%, Sigma-Aldrich), and pyridine (≥99.0%, "GR ACS" grade, EMD) were all used as received. P3HT (93% RR, 52 kDa MW, 2.2 PDI) was purchased from Reike Metals. Tetramethylurea (TMU, 99%, Alfa Aesar) was distilled at atmospheric pressure under nitrogen before use, discarding *ca.* 5−10% of the residue in the distillation flask.

Synthesis of Native-Ligand CdSe Nanocrystals, CdSe(NL). The synthesis is based on literature methods.[33] In a typical synthesis, $CdCO_3$ (1.17 g, 6.79 mmol), stearic acid (10.0 g), and tri-*n*-octylphosphine oxide (TOPO, 10.0 g) were stirred at 100 °C under flowing nitrogen (1.5 h), then held at 360 °C (1 h) during which time the solution became transparent. With rapid stirring, TOP/TOPSe (0.77 g, 9.7 mmol of selenium previously dissolved in 10 mL, 22 mmol of TOP) was quickly injected (~4 s). Exactly 2 min after the start of injection, the flask was removed from the heating bath and the reaction was quenched *via* air-cooling.

The reaction product was split between three 45-mL centrifuge tubes and the reaction flask was rinsed with 6 mL of toluene added equally to each centrifuge tube. To this was added EtOH (20 mL/tube), and the mixture was centrifuged down (6000 rpm, 2 min), and then the supernatant was discarded. To wash the nanocrystals, the solid was redispersed in toluene (10 mL/tube), after which EtOH (20 mL/tube) was added as a flocculant, the mixture was centrifuged (6000 rpm, 1 min), and then the supernatant was discarded. This washing procedure was repeated twice. The final dispersion was made in 6 mL of toluene, which was passed through a 0.45 μm PTFE syringe filter to give the final product. The product was stored in the dark at 10 °C.

Pyridine-Exchange of CdSe Nanocrystals, CdSe(Py). A CdSe(NL) dispersion in toluene (100 mg CdSe; 1 mL) was added to 10 mL of pyridine in a 50-mL round-bottomed flask fitted with a small water-cooled condenser. The system was vigorously purged with nitrogen for ~10 min, and then introduced into an 80 °C oil bath with slow stirring and heated for several hours. After cooling, the dispersion was divided between two 45-mL centrifuge tubes. Pentane (40−42 mL per tube) was added, the mixture was centrifuged down (6000 rpm, 30 s), the supernatant was discarded, and either pyridine or CdSe-in-pyridine from previous tubes was immediately added in order to disperse the solid. The total volume of pyridine used for redispersion was 1−2 mL. The dispersion was centrifuged (4000 rpm, 2 min) and carefully decanted from the small precipitate of agglomerates to give the final product. The product was stored in the dark at 10 °C.

***tert*-Butylthiol-Exchange of CdSe Nanocrystals, CdSe(tBT).** CdSe(NL) (100 mg in 1 mL of toluene) was placed in a 45-mL centrifuge tube, an equal volume of TMU and tBT (2 mL) were added, and the mixture was allowed to sit in the dark for 30 min. For the first washing, 8 mL of methanol was added to flocculate before centrifugation (6000 rpm, 1 min). The colorless supernatant was discarded, and the nanocrystals were redispersed in TMU (2 mL). Following redispersion, tBT (1 mL) was added and the mixture was allowed to sit in the dark for 30 min after which time pentane (15 mL) was added to induce flocculation prior to centrifugation (6000 rpm, 1 min). This tBT washing was repeated three more times. After five tBT washings, the CdSe(tBT) nanocrystals were

dispersed in 1 mL of TMU, and the mixture was stirred very rapidly before bubbling nitrogen through the liquid for ~1 min to evaporate residual pentane. At this point, tBT (0.1 mL, as an antioxidant) was added and the mixture was centrifuged (6000 rpm, 1 min) before decanting off the supernatant from the very tiny mass of precipitated agglomerates. The dispersion was passed through a 0.45 μm PTFE syringe filter and then stored in the dark without signs of agglomeration.

Characterization. UV−vis spectra were acquired on a Shimadzu UV-1800 spectrophotometer, using a quartz cuvette for liquid samples or a borosilicate glass microscope slide substrate for films. TGA measurements were made on a TA Instruments TGA Q50 instrument, using sample sizes of 5−15 mg in an alumina crucible under a flowing nitrogen atmosphere. TGA samples were prepared by drying the colloid under flowing nitrogen at 80−100 °C for up to 90 min, then lightly crushing with a spatula. CV, DPV, and SEC experiments were conducted using a BASi Epsilon-EC potentiostat with a C3 cell stand. All measurements were done using dry, degassed acetonitrile under a nitrogen atmosphere. The supporting electrolyte, tetra-*n*-butylammonium hexafluorophosphate (TBAP, 98%, Sigma-Aldrich), was recrystallized from ethanol and stored in a desiccator after vacuum drying. Acetonitrile (HPLC grade, EMD) was purified using a VAC solvent purifier. ITO cuvette slides (Delta Technologies Ltd., Loveland, CO, 7 × 50 × 0.7 mm, 5−15 Ω) were cleaned prior to film casting by sequential sonication in detergent, water, tetrachloroethylene, isopropyl alcohol, and finally subjected to a 10 min UV−ozone treatment. For CV, DPV, and SEC experiments, a Pt wire counter-electrode and a Ag wire pseudo-reference-electrode were used. The Ag reference electrode was calibrated against the Fc/Fc^+ redox couple, and all potentials were reported relative to NHE. Film thicknesses were determined by X-ray reflectometry using samples spun-cast on glass slides under identical conditions to those used for device processing. Reflectometry was performed on a Rigaku Ultima IV diffractometer in parallel beam geometry (2-mm beam width) using Cu Kα radiation (λ = 1.54 Å), a reduced beam intensity (40 kV, 3 mA), no attenuator, 0−2° scan range, continuous scan mode, 0.02° step size, and 0.1° min^{-1} scan rate. Oscillation patterns were fit with Rigaku GRX software, taking care to accurately fit the oscillation period to ensure reliable film thicknesses.

PL Lifetime Studies. Time correlated single photon counting measurements (TCSPC, 22 ps time resolution) were performed using a R3809U-50 Hamamatsu PMT with a B&H SPC-630 module. The grating placed in the monochromator was blazed at 600 nm with 1200 g mm^{-1}. Samples were spun cast onto glass under conditions that produced optical densities between 0.1−0.2 au at the excitation wavelength. Photoluminescence lifetimes were measured by detecting the fluorescence decay of the films at 650 nm, after excitation at 400 nm (neat CdSe films) or 550 nm (P3HT and hybrid films). Data that appear in Figure 7 were measured using an excitation fluence of 3 $\mu J\ cm^{-2}$. These data were found to scale linearly with PL decay traces measured at two times this excitation fluence (6 $\mu J\ cm^{-2}$, see Supporting Information, Figure S10), suggesting that nonlinear effects due to exciton annihilation do not significantly contribute to the plotted data.

Device Fabrication. Devices were fabricated and tested in air. Aluminum shot (Al; Alfa Aesar, 99.999%) was purchased and used as received. Patterned ITO-coated glass substrates (10 Ω cm^{-2}, Thin Film Devices, Inc.) were sequentially cleaned by sonication in detergent, water, tetrachloroethylene, acetone, and isopropyl alcohol followed by 10 min of UV-ozone treatment. A layer of PEDOT:PSS (Baytron P VP AI 4083, filtered through a 0.45 μm PTFE syringe filter) was spun-cast onto the cleaned ITO and heated at 120 °C for 30 min under vacuum (0.01 mmHg). Solutions of 10 mg mL^{-1} P3HT were prepared in *o*-dichlorobenzene, and were mixed with *o*-dichlorobenzene dispersions of CdSe to final concentrations of 22.5 mg mL^{-1} (2.5 mg mL^{-1} P3HT, 20 mg mL^{-1} CdSe), and were stirred for 12−18 h in the dark prior to use. CdSe(Py) dispersions required 5% pyridine as a cosolvent to prevent nanocrystal agglomeration. Likewise, CdSe(tBT) required 5% TMU as a cosolvent to prevent agglomeration. Active layers passed through 0.45 μm PTFE syringe filters were spun-cast in air onto annealed PEDOT:PSS layers (900 rpm, 45 s) forming films with thicknesses of 65−75 nm. Following spin-casting, active layer films were dried under a nitrogen atmosphere for 20 min before loading into a high vacuum (~2 μTorr) thermal deposition chamber (Kurt J. Lesker Co.) for Al deposition at a rate of 2 Å s^{-1}. Device active areas were 0.8 mm^2.

Device Characterization. Current-density dependence on applied test voltage measurements were performed under ambient conditions using a Keithley 2420 SourceMeter (sensitivity = 100 pA) in the dark and under ASTM G173−03 spectral mismatch corrected 1000 W m^{-2} white light illumination from an AM 1.5G filtered 300 W xenon arc lamp (Newport Oriel). Chopped and filtered monochromatic light (250 Hz, 10 nm fwhm) from a Cornerstone 260 1/4 M double grating monochromator (Newport 74125) was used in conjunction with an EG&G 7220 lock-in amplifier to perform all spectral responsivity measurements.

Conflict of Interest: The authors declare no competing financial interest.

Acknowledgment. This work was supported as part of the Center for Energy Nanoscience, an Energy Frontier Research Center funded by the U.S. Department of Energy, Office of Science, Office of Basic Energy Sciences under Award Number DE-SC0001013. R.L.B. also acknowledges the Research Corporation for Science Advancement for a Cottrell Scholar Award. The authors would like to thank Drs. S. T. Roberts and E. Couderc for careful proofreading of the manuscript and Profs. B. Thompson and M. Thompson for use of their testing facilities.

Supporting Information Available: UV−vis and PL spectra of nanocrystal dispersions, CV of P3HT films, DPV of nanocrystal films, dark *I*−*V* curves for hybrid P3HT:CdSe solar cells, TEM, and AFM of P3HT:CdSe films, steady-state PL of neat polymer and hybrid P3HT:CdSe films, TCSPC of neat nanocrystals films, and TCSPC of neat P3HT and hybrid films at different excitation fluences. This material is available free of charge *via* the Internet at http://pubs.acs.org.

REFERENCES AND NOTES

1. Lunt, R. R.; Osedach, T. P.; Brown, P. R.; Rowehl, J. A.; Bulovic, V. Practical Roadmap and Limits to Nanostructured Photovoltaics. *Adv. Mater.* **2011**, *23*, 5712–5727.
2. Shaheen, S. E.; Ginley, D. S.; Jabbour, G. E. Organic-Based Photovoltaics: Toward Low-Cost Power Generation. *MRS Bull.* **2005**, *30*, 10–19.
3. Brabec, C. J.; Dyakonov, V.; Scherf, U. *Organic Photovoltaics: Materials, Device Physics, and Manufacturing Technologies*; Wiley-VCH: Weinheim, Germany, 2008.
4. Kippelen, B.; Bredas, J. Organic Photovoltaics. *Energy Environ. Sci.* **2009**, *2*, 251–261.
5. Dennler, G.; Scharber, M. C.; Brabec, C. J. Polymer-Fullerene Bulk-Heterojunction Solar Cells. *Adv. Mater.* **2009**, *21*, 1323–1338.
6. Chen, D.; Nakahara, A.; Wei, D.; Nordlund, D.; Russell, T. P. P3HT/PCBM Bulk Heterojunction Organic Photovoltaics: Correlating Efficiency and Morphology. *Nano Lett.* **2011**, *11*, 561–567.
7. Green, M. A.; Emery, K.; Hishikawa, Y.; Warta, W. Solar Cell Efficiency Tables (version 37). *Prog. Photovolt. Res. Appl.* **2011**, *19*, 84–92.
8. Moule, A. J.; Chang, L.; Thambidurai, C.; Vidu, R.; Stroeve, P. Hybrid Solar Cells: Basic Principles and the Role of Ligands. *J. Mater. Chem.* **2012**, *22*, 2351–2368.
9. Cozzoli, P. D.; Pellegrino, T.; Manna, L. Synthesis, Properties and Perspectives of Hybrid Nanocrystal Structures. *Chem. Soc. Rev.* **2006**, *35*, 1195–1208.
10. McGehee, M. D. Nanostructured Organic−Inorganic Hybrid Solar Cells. *MRS. Bull.* **2009**, *34*, 95–100.
11. Habas, S. E.; Platt, H. A. S.; Van Hest, M. F. A. M.; Ginley, D. S. Low-Cost Inorganic Solar Cells: From Ink to Printed Device. *Chem. Rev.* **2010**, 6571–6594.

12. Xu, T.; Qiao, Q. Conjugated Polymer−Inorganic Semiconductor Hybrid Solar Cells. *Energy Environ. Sci.* **2011**, *4*, 2700–2720.
13. Sharma, S. N.; Sharms, H.; Singh, G.; Shivaprasad, S. M. Studies of Interaction of Amines with TOPO/TOP Capped CdSe Quantum Dots: Role of Crystallite Size and Oxidation Potential. *Mater. Chem. Phys.* **2008**, *110*, 471–480.
14. Querner, C.; Reiss, P.; Sadki, S.; Zagorska, M.; Pron, A. Size and Ligand Effects on the Electrochemical Responses of CdSe Nanocrystals. *Phys. Chem. Chem. Phys.* **2005**, *7*, 3204–3209.
15. Scharber, M. C.; Muhlbacher, D.; Koppe, M.; Denk, P.; Waldauf, C.; Heeger, A. J.; Brabec, C. J. Design Rules for Donors in Bulk-Heterojunction Solar Cells—Towards 10% Energy-Conversion Efficiency. *Adv. Mater.* **2006**, *18*, 789–794.
16. Huynh, W. U.; Dittmer, J. J.; Alivisatos, A. P. Hybrid Nanorod−Polymer Solar Cells. *Science* **2002**, *295*, 2425–2427.
17. Sun, B.; Greenham, N. C. Improved Efficiency of Photovoltaics Based on CdSe Nanorods and Poly(3-hexylthiophene) Nanofibers. *Phys. Chem. Chem. Phys.* **2006**, *8*, 3557–3560.
18. Gur, I.; Fromer, N. A.; Chen, C. P.; Kanaras, A. G.; Alivisatos, A. P. Hybrid Solar Cells with Prescribed Nanoscale Morphologies Based on Hyperbranched Semiconductor Nanocrystals. *Nano Lett.* **2007**, *7*, 409–414.
19. Talapin, D. V.; Lee, J. S.; Kovalenko, M. V.; Shevchenko, E. V. Prospects of Colloidal Nanocrystals for Electronic and Optoelectronic Applications. *Chem. Rev.* **2010**, *110*, 389–458.
20. Dayal, S.; Reese, M. O.; Ferguson, A. J.; Ginley, D. S.; Rumbles, G.; Kopidakis, N. The Effect of Nanoparticle Shape on the Photocarrier Dynamics and Photovoltaic Device Perfromance of Poly(3-hexylthiophene):CdSe Nanoparticle Bulk Heterojunction Solar Cells. *Adv. Funct. Mater.* **2010**, *16*, 2629–2635.
21. Dayal, S.; Kopidakis, N.; Olson, D. C.; Ginley, D. S.; Rumbles, G. Photovoltaic Devices with a Low Band Gap Polymer and CdSe Nanostructures Exceeding 3% Efficiency. *Nano Lett.* **2010**, *10*, 239–242.
22. Jeltsch, K. F.; Schadel, M.; Bonekamp, J. B.; Niyamakom, P.; Rauscher, F.; Lademann, H. W. A.; Dumsch, I.; Allard, S.; Scherf, U.; Meerholz, K. Efficiency Enhanced Hybrid Solar Cells Using a Blend of Quantum Dots and Nanorods. *Adv. Funct. Mater.* **2012**, *22*, 397–404.
23. Lefrancois, A.; Couderc, E.; Vincent, J. F.; Sadki, S.; Pron, A.; Reiss, P. Effect of the Treatment with Diamines and Dithiols on the Spectroscopic, Electrochemical and Electrical Properties of CdSe Nanocrystals' Thin Films. *J. Mater. Chem.* **2011**, *21*, 11524–11531.
24. Albero, J.; Martinez-Ferrero, E.; Iacopino, D.; Vidal-Ferran, A.; Palomares, E. Interfacial Charge Transfer Dynamics in CdSe/Dipole Molecules Coated Quantum Dot Polymer Blends. *Phys. Chem. Chem. Phys.* **2010**, *12*, 13047–13051.
25. Yang, S.; Prendergast, D.; Neaton, J. B. Tuning Semiconductor Band Edge Energies for Solar Photocatalysis *via* Surface Ligand Passivation. *Nano Lett.* **2012**, *12*, 383–388.
26. Munro, A. M.; Zacher, B.; Graham, A.; Armstrong, N. R. Photoemission Spectroscopy of Tethered CdSe Nanocrystals: Shifts in Ionization Potential and Local Vacuum Level as a Function of Nanocrystal Capping Ligand. *ACS Appl. Mater. Interfaces* **2010**, *2*, 863–869.
27. Zhou, Y.; Riehle, F. S.; Yuan, Y.; Schleiermacher, H. F.; Niggemann, M.; Urban, G. A.; Kruger, M. Improved Efficiency of Hybrid Solar Cells Based on Non-Ligand-Exchanged CdSe Quantum Dots and Poly(3-hexylthiophene). *Appl. Phys. Lett.* **2010**, *96*, 013304.
28. Zhou, Y.; Eck, M.; Kruger, M. Bulk-Heterojunction Hybrid Solar Cells Based on Colloidal Nanocrystals and Conjugated Polymers. *Energ. Environ. Sci.* **2010**, *3*, 1851–1864.
29. Radychev, N.; Lokteva, I.; Witt, F.; Kolny-Olesiak, J.; Borchert, H.; Parisi, J. Physical Origins of the Impact of Different Nanocrystal Surface Modifications on the Performance of CdSe/P3HT Hybrid Solar Cells. *J. Phys. Chem. C* **2011**, *115*, 14111–14122.
30. Zhou, Y.; Eck, M.; Veit, C.; Zimmermann, B.; Rauscher, F.; Niyamalom, P.; Yilmaz, S.; Dumsch, I.; Allard, S.; Scherf, U.; Kruger, M. Efficiency Enhancement for Bulk-Heterojunction Hybrid Solar Cells Based on Acid Treated CdSe Quantum Dots and Low Bandgap Polymer PCPDTBT. *Sol. Energy Mater. Sol. Cells* **2011**, *95*, 1232–1237.
31. Perez, M. D.; Borek, C.; Forrest, S. R.; Thompson, M. E. Molecular and Morphological Influences on the Open Circuit Voltages of Organic Photovoltaic Devices. *J. Am. Chem. Soc.* **2009**, *131*, 9281–9286.
32. Webber, D. H.; Brutchey, R. L. Ligand Exchange on Colloidal CdSe Nanocrystals Using Thermally Labile *tert*-Butylthiol for Improved Photocurrent in Nanocrystal Films. *J. Am. Chem. Soc.* **2012**, *134*, 1085–1092.
33. Yu, W. W.; Qu, L.; Guo, W.; Peng, X. Experimental Determination of the Extinction Coefficient of CdTe, CdSe, and CdS Nanocrystals. *Chem. Mater.* **2003**, *15*, 2854–2860.
34. Li, Y.; Zhong, H.; Li, R.; Zhou, Y.; Yang, C.; Li, Y. High-Yield Fabrication and Electrochemical Characterization of Tetrapodal CdSe, CdTe, and $CdSe_xTe_{1-x}$ Nanocrystals. *Adv. Funct. Mater.* **2006**, *16*, 1705–1716.
35. Baumgardner, W. J.; Choi, J. J.; Lim, Y. F.; Hanrath, T. SnSe Nanocrystals: Synthesis, Structure, Optical Properties, and Surface Chemistry. *J. Am. Chem. Soc.* **2010**, *132*, 9519–9521.
36. Cardona, C. M.; Li, W.; Kaifer, A. E.; Stockdale, D.; Bazan, G. C. Electrochemical Considerations for Determining Absolute Frontier Orbital Energy Levels of Conjugated Polymers for Solar Cell Applications. *Adv. Mater.* **2011**, *23*, 2367–2371.
37. Bard, Allen J., Larry, R. Faulkner. *Electrochemical Methods: Fundamentals and Applications*; John Wiley: New York, 2001.
38. Kucar, E.; Bucking, W.; Giernoth, R.; Nann, T. Determination of Defect States in Semiconductor Nanocrystals by Cyclic Voltammetry. *J. Phys. Chem. B* **2005**, *109*, 20355–20360.
39. Wang, C.; Shim, M.; Guyot-Sionnest, P. Electrochromic Nanocrystal Quantum Dots. *Science* **2001**, *291*, 2390–2392.
40. Araci, Z. O.; Shallcross, C. R.; Armstrong, N. R.; Saavedra, S. S. Potential-Modulated Attenuated Total Reflectance Characterization of Charge Injection Processes in Monolayer-Tethered CdSe Nanocrystals. *J. Phys. Chem. Lett.* **2010**, *1*, 1900–1905.
41. Potscavage, W. J.; Yoo, S.; Kippelen, B. Origin of the Open-Circuit Voltage in Multilayer Heterojunction Organic Solar Cells. *Appl. Phys. Lett.* **2008**, *93*, 193308.
42. Soreni-Harari, M.; Yaacobi-Gross, N.; Steiner, D.; Aharoni, A.; Banin, U.; Millo, O.; Tessler, N. Tuning Energetic Levels in Nanocrystal Quantum Dots through Surface Manipulations. *Nano Lett.* **2008**, *8*, 678–684.
43. Jasieniak, J; Califano, M.; Watkins, S. E. Size-Dependent Valence and Conduction Band-Edge Energies of Semiconductor Nanocrystals. *ACS Nano* **2011**, *5*, 5888–5902.
44. Vilan, A.; Shanzer, A.; Cahen, D. Molecular Control over Au/GaAs Diodes. *Nature* **2000**, *404*, 166–168.
45. Wuister, S. F.; Donega, C. M.; Meijerink, A. Influence of Thiol Capping on the Exciton Luminescence and Decay Kinetics of CdTe and CdSe Quantum Dots. *J. Phys. Chem. B* **2004**, *108*, 17393–17397.
46. Li, Z.; Gao, F.; Greenham, N. C.; McNeill, C. Comparison of the Operation of Polymer/Fullerene, Polymer/Polymer, and Polymer/Nanocrystal Solar Cells: A Transient Photocurrent and Photovoltage Study. *Adv. Funct. Mater.* **2011**, *21*, 1419–1431.
47. Noone, K. M.; Subramaniyan, S.; Zhang, Q.; Cao, G.; Jenejhe, S. A.; Ginger, D. S. Photoinduced Charge Transfer and Polaron Dynamics in Polymer and Hybrid Photovoltaic Thin Films: Organic *vs* Inorganic Acceptors. *J. Phys. Chem. C* **2011**, *115*, 24403–24410.